

## Local atomic structure of $K_xNa(1-x)NbO_3$ by total x-ray diffraction

Shashaank Gupta, Valeri Petkov, and Shashank Priya

Citation: *Applied Physics Letters* **105**, 232902 (2014); doi: 10.1063/1.4903512

View online: <http://dx.doi.org/10.1063/1.4903512>

View Table of Contents: <http://scitation.aip.org/content/aip/journal/apl/105/23?ver=pdfcov>

Published by the [AIP Publishing](#)

---

### Articles you may be interested in

[Polarization reversal and dynamic scaling of  \$\(Na\_{0.5}K\_{0.5}\)NbO\_3\$  lead-free ferroelectric ceramics with double hysteresis-like loops](#)

*J. Appl. Phys.* **112**, 104114 (2012); 10.1063/1.4768270

[A monoclinic-tetragonal ferroelectric phase transition in lead-free  \$\(K\_{0.5}Na\_{0.5}\)NbO\_3-x\%LiNbO\_3\$  solid solution](#)

*J. Appl. Phys.* **111**, 103503 (2012); 10.1063/1.4716027

[Piezoresponse and ferroelectric properties of lead-free  \$\[Bi\_{0.5}\(Na\_{0.7}K\_{0.2}Li\_{0.1}\)\_{0.5}\]TiO\_3\$  thin films by pulsed laser deposition](#)

*Appl. Phys. Lett.* **92**, 222909 (2008); 10.1063/1.2938364

[Giant strain in lead-free piezoceramics  \$Bi\_{0.5}Na\_{0.5}TiO\_3 - BaTiO\_3 - K\_{0.5}Na\_{0.5}NbO\_3\$  system](#)

*Appl. Phys. Lett.* **91**, 112906 (2007); 10.1063/1.2783200

[Electrical domain fixing of photorefractive index gratings in  \$\(K\_{0.5}Na\_{0.5}\)\_{0.2}\(Sr\_{0.75}Ba\_{0.25}\)\_{0.9}Nb\_2O\_6\$  crystals](#)

*Appl. Phys. Lett.* **77**, 1206 (2000); 10.1063/1.1289492

---



## Local atomic structure of $K_xNa_{(1-x)}NbO_3$ by total x-ray diffraction

Shashaank Gupta,<sup>1</sup> Valeri Petkov,<sup>2</sup> and Shashank Priya<sup>1,a)</sup>

<sup>1</sup>Center for Energy Harvesting Materials and Systems (CEHMS), Virginia Tech, Blacksburg, Virginia 24061, USA

<sup>2</sup>Department of Physics, Central Michigan University, Mount Pleasant, Michigan 48859, USA

(Received 15 October 2014; accepted 22 November 2014; published online 8 December 2014)

Local atomic structure of  $K_xNa_{(1-x)}NbO_3$  with  $0.0 \leq x \leq 1.0$  was studied using atomic Pair Distribution Function analysis based on x-ray diffraction. Powdered crystals were found to exhibit a re-entrant behavior by being orthorhombic (*Amm2*) for  $x < 0.42$ , monoclinic (*Pm*) for  $0.42 \leq x \leq 0.63$  and again orthorhombic (*Amm2*) for  $x > 0.63$ . Non-centrosymmetric structure of  $NaNbO_3$  (*Amm2*) was also evident in the piezoresponse force microscopy analysis revealing the presence of the ferroelectric domains and switching behavior. Lowering of the crystallographic symmetry for  $0.42 \leq x \leq 0.63$  is discussed in terms of differences in the sizes of  $Na^+$  and  $K^+$  ions and Na–O and K–O bond lengths. Besides being a bridging phase, as suggested by the previous studies on lead-based compositions, present study suggests that lower symmetry monoclinic phase of compositionally disordered perovskite solid solutions could also be a manifestation of the difference in the sizes of constituent ions and bond lengths. © 2014 AIP Publishing LLC.

[<http://dx.doi.org/10.1063/1.4903512>]

Morphotropic phase boundaries (MPBs) in distorted perovskite solid solutions are of enormous scientific interest due to the high piezoelectric and ferroelectric activities in their vicinity.<sup>1,2</sup> A number of perovskite solid solutions e.g.  $PbZrO_3$ - $PbTiO_3$  (PZT),  $Pb(Mg_{1/3}Nb_{2/3})O_3$ - $PbTiO_3$  (PMN-PT),  $Pb(Zn_{1/3}Nb_{2/3})O_3$ - $PbTiO_3$  (PZN-PT),  $Na_{0.5}Bi_{0.5}TiO_3$ - $BaTiO_3$  (NBT-BT) and  $KNbO_3$ - $NaNbO_3$  (KNN) exhibit higher functional properties at their respective MPBs.<sup>2–6</sup> The discovery of the lower symmetry monoclinic ( $M_A$  and  $M_C$  respectively) phase at MPBs in lead-based perovskites such as PZT and PMN-PT has attracted significant interest.<sup>4–10</sup> This monoclinic ( $M_A/M_C$ ) phase appearing at MPB was suggested to be the required bridging phase for the rotation of the polarization vector between rhombohedral (R) and tetragonal (T) symmetries, as illustrated in Figure 1. Higher piezoelectric and ferroelectric properties of MPB compositions were attributed to the ability of polarization vector to rotate in the fixed plane for the monoclinic phase, in contrast to its fixed direction for the higher symmetry end members (R and T).<sup>3–5,8,9,11</sup>

Glazer *et al.* proposed an alternative viewpoint that all the three long-range crystal structures reported across the MPB in PZT (rhombohedral, monoclinic and tetragonal) can be considered as the manifestation of a local monoclinic phase.<sup>12</sup> It was suggested that for the compositions well outside the MPB, the size of the monoclinic regions is smaller than the coherence length accessible by the conventional x-ray diffraction and thus is seen in diffuse scattering only. Hence, the sharp Bragg peaks in conventional x-ray crystallography yield “averaged out” structures with rhombohedral and tetragonal symmetries on two sides of MPB. On the other hand, due to the reduction in the bond valence sum at MPB, the size of the short-range ordered monoclinic domains/regions becomes larger than the coherence length

accessible by the conventional x-ray diffraction and hence the crystal structure with the monoclinic symmetry is detected clearly. In this scenario, the presence of a MPB in the phase diagrams of perovskite solid solutions would cease to exist locally.<sup>12</sup> Transmission electron microscopy studies performed on a number of PZT compositions have shown the minimum diffuse scattering at MPB, which are well consistent with the proposed phenomenon.<sup>12</sup>

Interestingly, all the previous studies investigating the correlation between the long and short-range atomic ordering and their effect on the functional properties have focused on MPBs existing between T and R symmetries in the lead-based perovskites.<sup>12,14</sup> Both the arguments explaining the existence of the monoclinic phase at MPBs as (i) the required bridging phase between R and T end members, and (ii) the transformation of the otherwise short range monoclinic phase to the long range one due to the decreased bond valence sum, have been found to be consistent with the experimental findings in R-T MPB compositions.<sup>4,6,8–10,12</sup> In order to shed light on the origin of the monoclinic phase at MPB, it would be beneficial to study a system other than R-T one in which the polarization rotation through bridging monoclinic phase is not desired (Figure 1). In such a scenario, the first point of view explaining the monoclinic phase as a desired bridging phase can be ruled out and hence, it would be interesting to see if the monoclinic phase still persists at local-scale for MPB compositions.

In this study, we investigate the evolution of the local atomic ordering in sodium potassium niobate ( $K_xNa_{(1-x)}NbO_3$ ) powders obtained from the grinding of the single crystals with  $0.0 \leq x \leq 1.0$ . In contrast to the previous studies on lead-based solid solutions comprising of end members belonging to R and T symmetries, the two end members of KNN ( $KNbO_3$  and  $NaNbO_3$ ) exhibit the orthorhombic (O) symmetry, though there has been some debate over the most relevant space group for  $NaNbO_3$ .<sup>13,15–17</sup> KNN solid solutions have been well studied for their long-range crystallographic nature and functional properties.<sup>1,2,18,19</sup> There is a wide

<sup>a)</sup>Author to whom correspondence should be addressed. Electronic mail: [spriya@vt.edu](mailto:spriya@vt.edu)

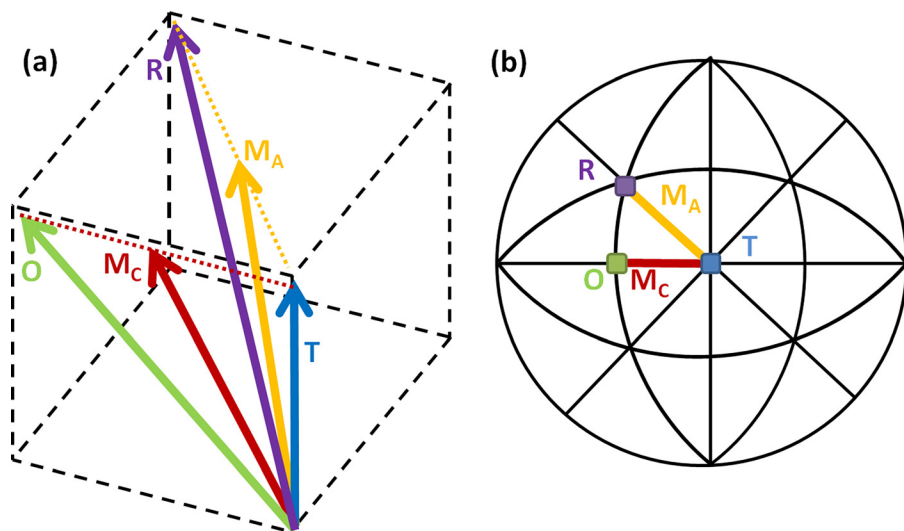


FIG. 1. Orientations of polarization vectors for different crystal structures (a) in pseudo-cubic unit cell and (b) stereographic projection.

consensus over the presence of MPB at  $x=0.5$ , where enhanced piezoelectric and ferroelectric activities are observed.<sup>2,18</sup> In spite of the fact that no polarization rotation is required through the bridging phase between the end members of O symmetry, a sequence of structural transformations take place at the macro-scale with the variation in composition.<sup>2,18,19</sup> Hence, it would be interesting to determine the sequence of the local structural transformations across the composition range ( $0 \leq x \leq 1$ ).

$K_xNa_{(1-x)}NbO_3$  crystals with target compositions  $x = 0, 0.2, 0.4, 0.5, 0.6, 0.8$  and  $1.0$  were grown by the flux method, described in detail elsewhere.<sup>2,20</sup> After growth, crystals were subjected to annealing at  $1000^\circ\text{C}$  for 2 h to remove any compositional non-homogeneity. To confirm the composition prior to crystallographic analysis, crystals were subjected to the energy dispersive X-ray spectroscopy (EDX). True compositions of the crystals were determined to be  $x = 0.0, 0.16, 0.42, 0.52, 0.63, 0.82$  and  $1.0$  respectively, which were close to the target compositions. Crystals were crushed into fine powder particles before being subjected to the local-scale crystallographic analysis using x-ray pair distribution function (PDF) analysis. Analysis of the diffuse scattered radiations along with Bragg scattered x-rays in PDF technique gives the advantage of revealing the short range order in crystalline materials.<sup>21,22</sup> Scattered X-ray intensities ( $I$ ) were measured for all the compositions mentioned above as a function of  $2\theta$  in the range of  $1^\circ$ – $120^\circ$  (angle between the incident and scattered radiation) with x-rays produced by silver anode tube. Since higher statistical accuracy is required for PDF analysis as compared to conventional crystallography, longer data collection time of the order of 48 h per sample was employed.

Raw diffraction data were corrected for sample absorption and background scattering and then reduced to the structure factors  $S(Q)$  defined in Eq. (1). In this equation,  $Q$  is the magnitude of the wave vector, which is related to the scattering angle  $2\theta$  and wavelength of radiation  $\lambda$  as  $Q = 4\pi \sin \theta / \lambda$ .

$$S(Q) = 1 + \left[ I^{\text{coh}}(Q) - \sum c_i |f_i(Q)|^2 \right] / \left| \sum f_i(Q) c_i \right|^2, \quad (1)$$

where  $c_i$  and  $f_i(Q)$  are the atomic concentration and structure factor for the atomic species of  $i^{\text{th}}$  type. The scattering

structure factors  $S(Q)$  were Fourier transformed as described in Eq. (2) to obtain the so-called PDFs ( $G(r)$ )

$$G(r) = \frac{2}{\pi} \int_0^{Q_{\text{max}}} Q [S(Q) - 1] \sin(Qr) dQ. \quad (2)$$

Experimental PDFs obtained for different compositions are shown in Figures 2 and 3. In these figures, black dots represent the experimentally measured data, while the continuous red lines are the best fits to them. As can be seen, calculated PDFs show good agreement with those determined experimentally. Small differences in the amplitude and width for few PDF peaks could be attributed to the errors arising from the approximations made for thermal motion of ions at room temperature. The radial distance range of  $40 \text{ \AA}$  corresponds to  $\sim 10$  pseudo-cubic unit cells in perovskites and well represents the average local structure. In typical atomic PDFs  $G(r)$  for perovskites, the first three peaks appearing at  $1.6$ – $2.4 \text{ \AA}$ ,  $2.5$ – $3.2 \text{ \AA}$  and  $3.2$ – $3.7 \text{ \AA}$  reflect the distinct B–O, A–O/O–O and A–B bond lengths respectively.<sup>21</sup> The disordered perovskites having more than one type of A/B cations can show the splitting of the PDF peaks due to the different bond lengths between the ions.

Figures 2(a) and 2(b) show the PDF data for the two end members:  $\text{NaNbO}_3$  ( $x=0.0$ ) and  $\text{KNbO}_3$  ( $x=1.0$ ) respectively. PDF data for  $\text{NaNbO}_3$  ( $x=0.0$ ) was found to have best fit with a model based on the orthorhombic space group  $Amm2$  with two formula units per cell ( $Z=2$ ) and refined lattice parameters were found to be  $a = 3.890 \text{ \AA}$ ,  $b = 5.512 \text{ \AA}$  and  $c = 5.519 \text{ \AA}$ . This finding for  $\text{NaNbO}_3$  is in contrast with another recent neutron diffraction PDF study suggesting space group to be non-centrosymmetric  $R3c$  for  $r < 5 \text{ \AA}$  and centrosymmetric  $Pbcm$  for  $r > 5 \text{ \AA}$  in the temperature range of  $300 \text{ K}$ – $490 \text{ K}$ .<sup>16</sup> Investigation at  $15 \text{ K}$  performed in the same study suggested a coexistence of  $Pbcm$  and  $R3c$  space groups at  $r > 10 \text{ \AA}$ , while below this length scale PDF data gave best fit for  $R3c$  space group. The discrepancy regarding the room temperature local structure in two studies could be due to the different length scales at which the structure was averaged.<sup>16</sup> One of the early investigations performed on  $\text{NaNbO}_3$  single crystals also suggested the coexistence of a ferroelectric phase

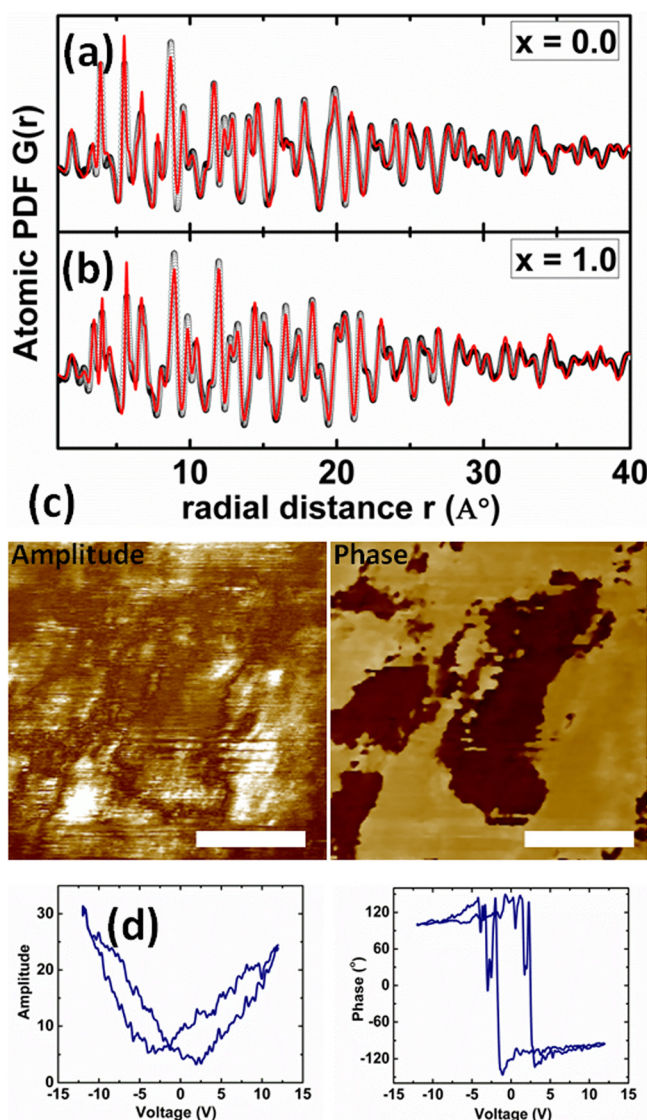


FIG. 2. Experimental (black dots) and model fit (lines in red) PDFs for (a)  $\text{NaNbO}_3$ , (b)  $\text{KNbO}_3$ , (c) PFM amplitude and phase contrast images (scale bars represent  $2\ \mu\text{m}$ ) and (d) piezoelectric switching loops obtained for  $\text{NaNbO}_3$ .

with the antiferroelectric one at room temperature, though the reproducibility of the ferroelectric phase was found to be dubious.<sup>23</sup> Studies intended to experimentally determine the ferroelectric nature of  $\text{NaNbO}_3$  have seen divergence in the conclusion.<sup>24,25</sup> It was suggested that the free energy for two phases are very close to each other at room temperature and by applying a small electric field, antiferroelectric phase can easily be transformed to the ferroelectric one.<sup>15,23</sup>

In addition to the crystallographic analysis, polarization switching behavior of  $\text{NaNbO}_3$  can shed an extra light on its ferroelectric nature. Piezoresponse force microscopy (PFM) was conducted on  $(100)_{\text{pc}}$  oriented  $\text{NaNbO}_3$  crystal. Presence of the ferroelectric domains can be seen in the amplitude and phase contrast images, as shown in Figure 2(c). A triangular electric signal of amplitude  $\pm 12\ \text{V}$  was used to confirm the local-switching behavior. Amplitude and phase angle loops shown in Figure 2(d) further confirm the local non-zero piezoelectric response of  $\text{NaNbO}_3$  and hence are consistent with the non-centrosymmetric  $Amm2$  space group. The experimental

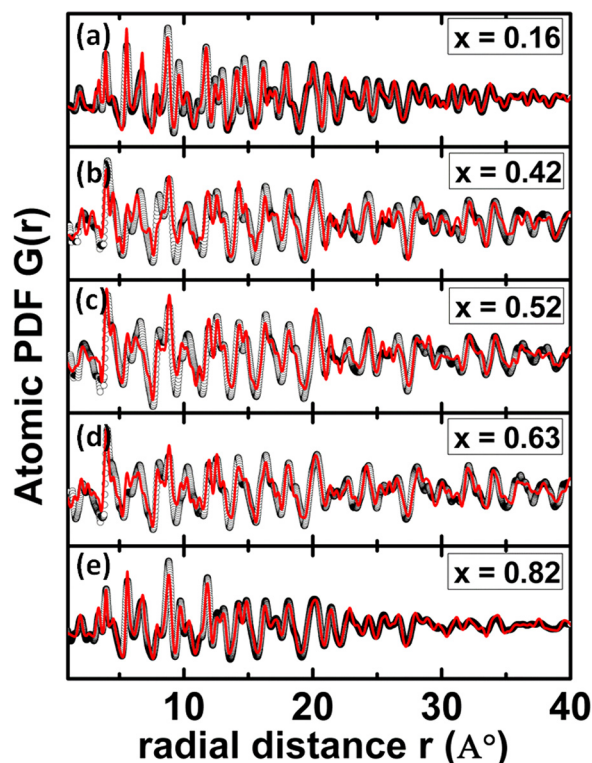


FIG. 3. Experimental (black dots) and model fit (lines in red) PDFs for KNN with (a)  $x = 0.16$ , (b)  $0.42$ , (c)  $0.52$ , (d)  $0.63$  and (e)  $0.82$ .

PDF for  $\text{KNbO}_3$  ( $x = 1.0$ ) was also best fit with the structure model based on the orthorhombic  $Amm2$  space group having two formula units ( $Z = 2$ ) per cell. The result suggests a local-scale ordering in  $\text{KNbO}_3$  being similar to its average structure reported previously.<sup>18</sup> PDF-refined lattice parameters for  $\text{KNbO}_3$  were found to be  $a = 3.971\ \text{Å}$ ,  $b = 5.701\ \text{Å}$  and  $c = 5.671\ \text{Å}$ .

Figure 3 shows the experimental PDFs for samples with  $x = 0.16, 0.42, 0.52, 0.63$  and  $0.82$ . Among these, the samples with  $x = 0.16$  and  $0.82$  had the lowest compositional disorder and they maintain the orthorhombic  $Amm2$  space group of the end members  $\text{NaNbO}_3$  and  $\text{KNbO}_3$ . The increased local compositional disorder for  $x = 0.42, 0.52$  and  $0.63$  resulted in the modification of the structure to monoclinic  $Pm$ . PDF-refined lattice parameters of the pseudocubic monoclinic unit cells (one formula unit per cell) for different samples ( $x = 0.42, 0.52$  and  $0.63$ ) are listed in Table I. The orthorhombic and monoclinic unit cells can be transformed to each other by using the relations  $a_o = 2a_m \sin(\beta/2)$ ,  $b_o = 2b_m \sin(\beta/2)$  and  $c_o = c_m$ .<sup>26</sup> Though in the present case, it is important to note that the transformation of  $Amm2$  to  $Pm$  symmetry for  $0.42 \leq x \leq 0.63$  is due to the loss of some of the symmetry elements of the former. The transformation from  $Amm2 \rightarrow Pm$  suggests a loss of mirror plane normal to  $[100]$  and a two-fold axis along  $[001]$ . Since in this case both the end compositions ( $x \geq 0.63$  and  $x \leq 0.42$ ) are orthorhombic in nature, there is no such requirement of a lower symmetry bridging phase (Figure 1).<sup>3-6,8-10</sup> The phenomenon of local lowering of space group symmetry has been demonstrated previously as well for a number of non-perovskite solid solutions with higher symmetry end members.<sup>27,28</sup>

TABLE I. Lattice parameters and space groups determined for different KNN compositions.

x	a (Å)	b (Å)	c (Å)	$\alpha$ (°)	$\beta$ (°)	$\gamma$ (°)	Space group
0.0	3.89(1)	5.51(1)	5.52(1)	90	90	90	<i>Amm2</i>
0.16	3.93(1)	5.54(1)	5.54(1)	90	90	90	<i>Amm2</i>
0.42	3.97(1)	3.97(1)	3.92(1)	90	90.6(1)	90	<i>Pm</i>
0.52	3.98(1)	3.99(1)	3.92(1)	90	90.4(1)	90	<i>Pm</i>
0.63	3.97(1)	3.98(1)	3.92(1)	90	90.9(1)	90	<i>Pm</i>
0.82	3.98(1)	5.68(1)	5.58(1)	90	90	90	<i>Amm2</i>
1.0	3.97(1)	5.70(1)	5.67(1)	90	90	90	<i>Amm2</i>

Lowering of symmetry in compositionally disordered KNN solid solutions can be understood as a consequence of the difference in the sizes of  $\text{Na}^+$  and  $\text{K}^+$  ions along with highly rigid and distinct lengths of Na–O and K–O bonds.<sup>27,29</sup> The radius of  $\text{K}^+$  is about 1.64 Å as compared to 1.39 Å for  $\text{Na}^+$ .<sup>30</sup> Similarly, Na–O and K–O bonds in the respective end members  $\text{NaNbO}_3$  and  $\text{KNbO}_3$  have the lengths of 2.12 Å and 2.82 Å respectively. This difference in bond lengths amounts for the variation of about 33% in the length of A–O bonds in the composition range of  $0.0 \leq x \leq 1.0$ . According to the Vegard's law, bond lengths should vary linearly with composition to accommodate the varying size of constituent ions in order to maintain the overall symmetry of the end compositions.<sup>31,32</sup> Average bond lengths determined by conventional XRD obey Vegard's law in the case of several solid solutions, including perovskites.<sup>31,33,34</sup> Though, experimental as well as theoretical studies have revealed that this phenomenon is limited only to the averaged bond lengths, locally bond lengths do not follow such behavior.<sup>27,28,31</sup> Small or no variation in bond lengths in solid solutions could be attributed to the high energy penalty for altering the bond lengths between two atoms.<sup>27</sup> In this scenario, rotations of bonds is expected to take place in order to accommodate the difference in sizes of substituting ions and hence loss of some of the symmetry elements. As described above, loss of the mirror plane and two-fold rotation axis in KNN results in the transformation  $Amm2 \rightarrow Pm$ .

Moreover, contrary to the findings of the previous reports, there ceases to be the existence of a MPB in the composition range of  $0.42 \leq x \leq 0.63$ . This observation is in agreement with the hypothesis of Glazer *et al.* in case of PZT, suggesting the transformation between R and T crystal symmetries via a local monoclinic phase without passing through any MPB.<sup>12</sup> Existence of the monoclinic symmetry at local-scale while its transformation to the orthorhombic one on K-rich side could be due to the interplay of valence bond sum between short- and long-range ordering.<sup>12,18,19</sup>

Figure 4 shows the variation of the volume of pseudo-cubic unit cell (volume per formula unit of  $\text{ABO}_3$ ) with the composition of KNN. Along with the local-scale pseudo-cubic unit cell volume determined in this study, averaged unit cell volumes were calculated by using lattice parameters found in previous studies.<sup>17,33</sup> The larger size  $\text{K}^+$  ions (1.64 Å) as compared to  $\text{Na}^+$  ions (1.39 Å)<sup>30</sup> results in an increase in the pseudo-cubic unit cell volume with increasing x. Notably, the variation of unit cell volume at short-range distance is more pronounced when the end members are

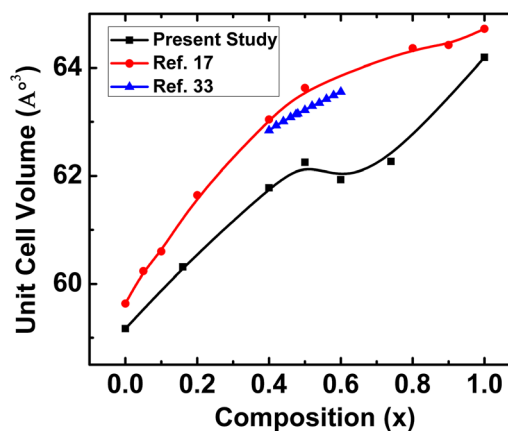


FIG. 4. Variation of the pseudo-cubic unit cell volume (volume occupied per formula unit) with KNN composition.

approached, whereas for  $0.42 \leq x \leq 0.63$  it remains almost constant. Conversion of two plots towards the ends ( $\text{NaNbO}_3$  and  $\text{KNbO}_3$ ) suggests that the completely ordered compositions have similar crystallographic nature at short- and long-range distances. This observation is consistent with our hypothesis that any dissimilarity in the local and average structures in  $0.42 \leq x \leq 0.63$  is primarily due to their high chemical disorder.

In summary, KNN single crystals in the composition range of  $0.0 \leq x \leq 1.0$  were investigated for their local-scale atomic structure. End members, with none or very low degree of disorder ( $x = 0.0, 0.16, 0.82$  and  $1.0$ ) were found to be orthorhombic with *Amm2* space group symmetry. Presence of the non-zero piezoresponse and hence non-centrosymmetric space group for  $\text{NaNbO}_3$  was evident by PFM. For highly disordered compositions ( $x = 0.42, 0.52$  and  $0.63$ ), locally the atomic structure was monoclinic with *Pm* space group symmetry. The lowering of the space group symmetry for highly disordered KNN compositions could be attributed to the interplay between bond length alteration and rotation to accommodate the A-site ions of two sizes. Hence, for perovskite solid solutions with crystallographically similar end members, lower symmetry monoclinic phase may still exist irrespective of the requirement of any bridging phase at MPB.

The authors gratefully acknowledge the financial support from Office of Basic Energy Sciences, Department of Energy through the Grant No. DE-FG02-07ER46480.

- <sup>1</sup>B. Jaffe, W. R. Cook, and H. L. Jaffe, *Piezoelectric Ceramics* (Academic Press, London, New York, 1971).
- <sup>2</sup>S. Gupta, S. Huband, D. S. Keeble, D. Walker, P. Thomas, D. Viehland, and S. Priya, *CrystEngComm* **15**(34), 6790–6799 (2013).
- <sup>3</sup>B. Noheda, Z. Zhong, D. E. Cox, G. Shirane, S. E. Park, and P. Rehrig, *Phys. Rev. B* **65**(22), 224101 (2002).
- <sup>4</sup>B. Noheda, D. E. Cox, G. Shirane, J. A. Gonzalo, L. E. Cross, and S.-E. Park, *Appl. Phys. Lett.* **74**(14), 2059–2061 (1999).
- <sup>5</sup>B. Noheda, D. E. Cox, G. Shirane, J. Gao, and Z. G. Ye, *Phys. Rev. B* **66**(5), 054104 (2002).
- <sup>6</sup>B. Noheda, *Curr. Opin. Solid State Mater. Sci.* **6**(1), 27–34 (2002).
- <sup>7</sup>D. La-Orautapong, B. Noheda, Z. G. Ye, P. M. Gehring, J. Toulouse, D. E. Cox, and G. Shirane, *Phys. Rev. B* **65**(14), 144101 (2002).
- <sup>8</sup>B. Noheda, D. E. Cox, G. Shirane, R. Guo, B. Jones, and L. E. Cross, *Phys. Rev. B* **63**(1), 014103 (2000).

- <sup>9</sup>B. Noheda, J. A. Gonzalo, L. E. Cross, R. Guo, S. E. Park, D. E. Cox, and G. Shirane, *Phys. Rev. B* **61**(13), 8687–8695 (2000).
- <sup>10</sup>B. Noheda, D. E. Cox, G. Shirane, S. E. Park, L. E. Cross, and Z. Zhong, *Phys. Rev. Lett.* **86**(17), 3891–3894 (2001).
- <sup>11</sup>J.-M. Kiat, Y. Uesu, B. Dkhil, M. Matsuda, C. Malibert, and G. Calvarin, *Phys. Rev. B* **65**(6), 064106 (2002).
- <sup>12</sup>A. M. Glazer, P. A. Thomas, K. Z. Baba-Kishi, G. K. H. Pang, and C. W. Tai, *Phys. Rev. B* **70**(18), 184123 (2004).
- <sup>13</sup>A. C. Sakowski-Cowley, K. Lukaszewicz, and H. D. Megaw, *Acta Crystallogr., Sect. B: Struct. Crystallogr. Cryst. Chem.* **25**(5), 851–865 (1969).
- <sup>14</sup>Y. M. Jin, Y. U. Wang, A. G. Khachatryan, J. F. Li, and D. Viehland, *Phys. Rev. Lett.* **91**(19), 197601 (2003).
- <sup>15</sup>S. K. Mishra, N. Choudhury, S. L. Chaplot, P. S. R. Krishna, and R. Mittal, *Phys. Rev. B* **76**(2), 024110 (2007).
- <sup>16</sup>L. Jiang, D. C. Mitchell, W. Dmowski, and T. Egami, *Phys. Rev. B* **88**(1), 014105 (2013).
- <sup>17</sup>G. Shirane, R. Newnham, and R. Pepinsky, *Phys. Rev.* **96**(3), 581 (1954).
- <sup>18</sup>D. W. Baker, P. A. Thomas, N. Zhang, and A. M. Glazer, *Appl. Phys. Lett.* **95**(9), 091903 (2009).
- <sup>19</sup>D. W. Baker, P. A. Thomas, N. Zhang, and A. M. Glazer, *Acta Crystallogr., Sect. B: Struct. Sci.* **65**(1), 22–28 (2009).
- <sup>20</sup>S. Gupta and S. Priya, *Appl. Phys. Lett.* **98**(24), 242906 (2011).
- <sup>21</sup>T. Egami and S. J. L. Billinge, *Underneath the Bragg Peaks: Structural Analysis of Complex Materials* (Pergamon, Kidlington, Oxford, United Kingdom; Boston, 2003).
- <sup>22</sup>V. Petkov, *Characterization of Materials* (John Wiley and Sons, Inc., 2002).
- <sup>23</sup>I. Lefkowitz, K. Lukaszewicz, and H. D. Megaw, *Acta Crystallogr.* **20**(5), 670–683 (1966).
- <sup>24</sup>T. Arioka, H. Taniguchi, M. Itoh, K. Oka, R. Wang, and D. Fu, *Ferroelectrics* **401**(1), 51–55 (2010).
- <sup>25</sup>Y. Shiratori, A. Magrez, K. Kasezawa, M. Kato, S. Röhrig, F. Peter, C. Pithan, and R. Waser, *J. Electroceram.* **19**(4), 273–280 (2007).
- <sup>26</sup>D. Viehland, *J. Appl. Phys.* **88**(8), 4794–4806 (2000).
- <sup>27</sup>V. Petkov, I. K. Jeong, J. S. Chung, M. F. Thorpe, S. Kycia, and S. J. L. Billinge, *Phys. Rev. Lett.* **83**(20), 4089–4092 (1999).
- <sup>28</sup>J. B. Boyce and J. C. Mikkelsen, *Phys. Rev. B* **31**(10), 6903–6905 (1985).
- <sup>29</sup>V. A. Shuvaeva, D. Zekria, A. M. Glazer, Q. Jiang, S. M. Weber, P. Bhattacharya, and P. A. Thomas, *Phys. Rev. B* **71**(17), 174114 (2005).
- <sup>30</sup>R. Shannon, *Acta Crystallogr., Sect. A: Cryst. Phys., Diffraction, Theor. Gen. Crystallogr.* **32**(5), 751–767 (1976).
- <sup>31</sup>I. Levin, E. Cockayne, M. W. Lufaso, J. C. Woicik, and J. E. Maslar, *Chem. Mater.* **18**(3), 854–860 (2006).
- <sup>32</sup>A. R. Denton and N. W. Ashcroft, *Phys. Rev. A* **43**(6), 3161–3164 (1991).
- <sup>33</sup>J. Tellier, B. Malic, B. Dkhil, D. Jenko, J. Cilensek, and M. Kosec, *Solid State Sci.* **11**(2), 320–324 (2009).
- <sup>34</sup>L. H. Brixner, *J. Inorg. Nucl. Chem.* **14**(3–4), 225–230 (1960).